THE INFLUENCE OF THE INLET SWIRL ON THE STRUCTURE OF INVISCID FLOWS IN PIPES

J. Ortega-Casanova and R. Fernández-Feria
Universidad de Málaga, E.T.S. Ingenieros Industriales, 29013 Málaga, SPAIN

ABSTRACT

The inviscid evolution along a pipe of varying radius of three different inlet swirling flows is analyzed by solving numerically the Bragg-Hawthorne equation. The downstream structure of the flow changes abruptly above certain threshold values of the swirl parameter (L). In particular, there exist a value L_r above which a near-wall region of flow reversal is formed downstream, and a critical value L_f above which the axial vortex breaks down. It is shown that the dependence upon the pipe geometry of these critical values of the swirl parameter varies strongly with the inlet azimutal velocity profile considered. The numerical results are compared with exact and approximate cylindrical solutions for the downstream flow, which yield the values L_r and L_f in excellent agreement with the numerical results.

INTRODUCTION

Swirling flows in pipes of different geometries have been extensively used as relatively simple models to analyze the phenomenon of vortex breakdown. In particular, a number of theoretical and numerical works have made use of the inviscid flow equations to explain the phenomenon (see, e.g., [1] for a review), arguing that vortex breakdown is essentially an inviscid phenomenon, and extrapolating this conclusion to more complex swirling flow configurations. The inviscid approach has the advantage of its simplicity, because the axisymmetric flow is governed by just a partial differential equation (see below). However, it has the drawback of the initial, or inlet flow, conditions, which can be chosen arbitrarily owing to the fact that any cylindrical velocity profile is a solution to the cylindrical Euler equations. Therefore, one may question how the inlet flow affects to the inviscid evolution of the flow, particularly to the breakdown of the downstream flow. In this work we choose a pipe geometry where the inlet flow conditions can be specified with precision if viscosity were taken into account, and follow the inviscid evolution of three different inlet swirling flows by solving numerically the Bragg-Hawthorne equation. The results show that the structure of the downstream flow changes when the inlet swirl parameter goes across some threshold values which depend on the flow geometry. However, it is shown that, depending on the inlet flow considered, these critical values of the swirl parameter are very different functions of the flow geometry. Further, some flow transitions may even disappear when a particular inlet flow is considered.

FORMULATION OF THE PROBLEM

Under the assumptions of incompressible, axisymmetric and steady flow of an inviscid fluid with velocity field (u, v, w) in cylindrical coordinates (r, θ, z), the stream function Ψ of the meridional motion,

$$u = -\frac{1}{r}\frac{\partial \Psi}{\partial z}, \quad w = \frac{1}{r}\frac{\partial \Psi}{\partial r}, \tag{1}$$

satisfies the Bragg-Hawthorne (B-H) equation [2],

$$\frac{\partial^2 \Psi}{\partial z^2} - \frac{1}{r}\frac{\partial \Psi}{\partial r} + \frac{\partial \Psi^2}{\partial r^2} = r^2 \frac{dH}{d\Psi} - C\frac{dC}{d\Psi}, \tag{2}$$

where $H(\Psi)$ and $C(\Psi)$ are the Bernoulli function and the circulation, respectively,

$$H = \frac{p}{\rho} + \frac{1}{2}(u^2 + v^2 + w^2), \quad C = rv, \tag{3}$$

with p the pressure field and ρ the fluid density. We are interested here in solving this equation inside a pipe with the form sketched in figure 1, with an outer wall contraction and a centre body inside.

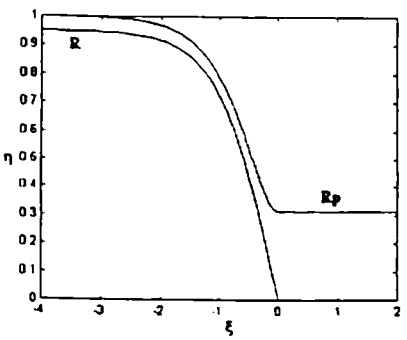

Figure 1. Pipe geometry.

6th Annual Conference of the CFD Society of Canada

The inner wall dies out at $z = 0$, and its non-dimensional radius is given by:

$$\eta_i(\xi) \equiv \frac{r_i(z)}{r_2} = R\tanh(-\alpha\xi) \text{ for } -\xi_1 \le \xi \le 0, \quad (4)$$

$$\eta_i(\xi) = 0 \text{ for } 0 < \xi \le \xi_2. \quad (5)$$

Here we have used the pipe inlet radius r_2 as the characteristic length, defining

$$\eta \equiv \frac{r}{r_2}, \ \xi \equiv \frac{z}{r_2}, \ R \equiv \frac{r_1}{r_2}, \quad (6)$$

where r_1 is the upstream radius of the inner wall of the pipe. α is a non-dimensional geometric parameter that characterizes the axial length of the inner wall. The radius of the outer wall, r_o, is defined in terms of r_i and the given interior section $\mathcal{S}(\xi) \equiv \frac{A(z)}{\pi r_2^2}$ of the pipe:

$$\eta_o(\xi) \equiv \frac{r_o(z)}{r_2} = \sqrt{\mathcal{S}(\xi) + \eta_i^2(\xi)}. \quad (7)$$

The particular forms of $\mathcal{S}(\xi)$ used in the computations are specified in the next section. The functions $H(\Psi)$ and $C(\Psi)$ are fixed by the velocity profiles at the pipe inlet, $\xi = -\xi_1$, $R \le \eta \le 1$, which are characterized by an axial velocity U and an angular velocity Ω. These parameters are used to define the non-dimensional velocity components as

$$\overline{u} \equiv \frac{u}{U}, \ \overline{v} \equiv \frac{v}{\Omega r_2}, \ \overline{w} \equiv \frac{w}{U}, \quad (8)$$

and a swirl parameter

$$L \equiv \frac{\Omega r_2}{U}. \quad (9)$$

We shall use three different inlet velocity profiles, denoted by (a), (b) and (c) in what follows:

$$(a)\ \overline{u} = 0, \ \overline{v} = \eta, \ \overline{w} = 1, \quad (10)$$

$$(b)\ \overline{u} = 0, \ \overline{v} = \frac{\eta^2 - R^2}{\eta(1-R^2)}, \ \overline{w} = 1, \quad (11)$$

$$(c)\ \overline{u} = 0, \ \overline{v} = \frac{R^2(1-\eta^2)}{\eta(1-R^2)}, \ \overline{w} = 1. \quad (12)$$

All of them correspond to a cylindrical ($u = 0$) flow with an uniform axial velocity ($w = U$). In relation to the azimutal velocity, the first profile corresponds to a rigid body rotation, with the two inlet pipe walls rotating at an angular velocity Ω; the second velocity profile corresponds to a rotation of the outer wall, with the inner wall at rest, and the third one to a rotation of the inner wall only. The corresponding pressure distributions at the pipe inlet are:

$$(a)\ \overline{p} = \frac{1}{2}\eta^2 + p_0, \quad (13)$$

$$(b)\ \overline{p} = \frac{1}{(1-R^2)^2}\left(\frac{\eta^2}{2} - \frac{R^4}{2\eta^2} - 2R^2\ln\eta\right) + p_0, \quad (14)$$

$$(c)\ \overline{p} = \frac{R^4}{(1-R^2)^2}\left(\frac{\eta^2}{2} - \frac{1}{2\eta^2} - 2\ln\eta\right) + p_0, \quad (15)$$

where the non-dimensional pressure has been defined as

$$\overline{p} \equiv \frac{p}{\rho(\Omega r_2)^2}, \quad (16)$$

and p_0 is a reference value.

In non-dimensional form, the B-H equation (2) may be written as

$$\psi_{\xi\xi} - \frac{1}{\eta}\psi_\eta + \psi_{\eta\eta} = 4L^2\left(\eta^2\frac{d\overline{H}}{d\psi} - \overline{C}\frac{d\overline{C}}{d\psi}\right), \quad (17)$$

where subscripts indicate differentiation and

$$\psi \equiv \frac{\Psi}{\frac{1}{2}Ur_2^2}, \ \overline{H} \equiv \frac{H}{\Omega^2 r_2^2}, \ \overline{C} \equiv \frac{C}{\Omega r_2^2}. \quad (18)$$

$\overline{H}$ and $\overline{C}$ are obtained from (10)-(15):

$$(a)\ \overline{H}(\psi) = \psi, \ \overline{C}(\psi) = \psi + R^2, \quad (19)$$

$$(b)\ \overline{H}(\psi) = \frac{1}{(1-R^2)^2}(\psi - R^2\ln(\psi + R^2)),$$

$$\overline{C}(\psi) = \frac{\psi}{1-R^2}, \quad (20)$$

$$(c)\ \overline{H}(\psi) = \frac{R^4}{(1-R^2)^2}(\psi - \ln(\psi + R^2)),$$

$$\overline{C}(\psi) = R^2\left(1 - \frac{\psi}{1-R^2}\right), \quad (21)$$

where an irrelevant additive constant in $\overline{H}$ has been omitted. The B-H equation (17) can be written in a compact form for the three inlet flow considered as

$$\psi_{\xi\xi} - \frac{1}{\eta}\psi_\eta + \psi_{\eta\eta} =$$

$$a^2\left(c_1\eta^2 - \psi + c_2 + \eta^2\frac{c_3\psi + c_4}{\psi + R^2}\right), \quad (22)$$

where the constants a, and c_i, $i = 1,2,3,4$, are given by

$$(a)\ c_1 = 1, \ c_2 = -R^2, \ c_3 = 0, \ c_4 = 0,$$

$$a = 2L, \quad (23)$$

$$(b)\ c_1 = 0, \ c_2 = 0, \ c_3 = 1, \ c_4 = 0,$$

$$a = \frac{2L}{1-R^2}, \quad (24)$$

$$(c)\ c_1 = 1, \ c_2 = 1 - R^2, \ c_3 = 0, \ c_4 = -1,$$

$$a = \frac{2LR^2}{1-R^2}. \quad (25)$$

Note that the (22) is linear only for the inlet flow corresponding to the case (a); for the cases (b) and (c) the equation is non-linear. This equation must be solved with the boundary conditions:

$$\psi(\eta = \eta_0, \xi) = 0, \quad -\xi_1 \le \xi \le \xi_2, \tag{26}$$

$$\psi(\eta = \eta_1, \xi) = 1 - R^2, \quad -\xi_1 \le \xi \le \xi_2, \tag{27}$$

$$\psi(\eta, \xi = -\xi_1) = \eta^2 - R^2, \quad R \le \eta \le 1, \tag{28}$$

$$\psi_{\xi\xi} = 0, \quad \xi = \xi_2, \quad 0 \le \eta \le R_p, \tag{29}$$

where

$$R_p = \frac{r_3}{r_2}, \tag{30}$$

and r_3 is the outlet radius of the pipe. The first two conditions indicate that the inner and outer wall are streamlines. The third comes from the uniform axial velocity at the pipe inlet, and the fourth indicates that the flow is cylindrical ($\overline{u}_\xi = \psi_{\xi\xi} = 0$) at the pipe outlet (see [3] for a discussion of other possible boundary conditions at the pipe outlet).

NUMERICAL RESULTS

To perform the numerical integration of (22)-(29) we shall firstly use a constant value for the interior section of the pipe $\mathcal{S}(\xi)$:

$$\mathcal{S}(\xi) \equiv \mathcal{S}_0 = 1 - R^2. \tag{31}$$

It is convenient to transform the fluid domain onto a rectangular one using the new radial coordinate

$$\sigma = \frac{\eta_i(\xi) - \eta}{\eta_i(\xi) - \eta_o(\xi)}, \tag{32}$$

so that the computational domain is

$$-\xi_1 \le \xi \le \xi_2 \text{ and } 0 \le \sigma \le 1. \tag{33}$$

With this transformation (17) becomes

$$\psi_{\xi\xi} + f_1\psi_{\xi\sigma} + f_2\psi_{\sigma\sigma} + f_3\psi_\sigma =$$

$$4L^2[\{\sigma(\eta_1 - \eta_0) + \eta_0\}^2 \frac{dH}{d\psi} - C\frac{dC}{d\psi}], \tag{34}$$

and the boundary conditions (26)-(29) may be written as

$$\psi(\sigma = 0, \xi) = 0, \quad -\xi_1 \le \xi \le \xi_2, \tag{35}$$

$$\psi(\sigma = 1, \xi) = 1 - R^2, \quad -\xi_1 \le \xi \le \xi_2, \tag{36}$$

$$\psi(\sigma, \xi = -\xi_1) = [\sigma(\eta_1 - \eta_0) + \eta_0]^2 - R^2, \quad 0 \le \sigma \le 1, \tag{37}$$

$$\psi_{\xi\xi} = 0, \quad \xi = \xi_2, \quad 0 \le \sigma \le 1. \tag{38}$$

In (34) the different functions $f_i(\xi, \sigma), i = 1, 2, 3$ are given by:

$$f_1 = 2\eta_i' \frac{1}{\eta_i - \eta_o} - [\eta_i' - \eta_o'] \frac{2\sigma}{\eta_i - \eta_o}, \tag{39}$$

$$f_2 = \frac{1}{(\eta_i - \eta_o)^2} + \frac{f_1^2}{4}, \tag{40}$$

$$f_3 = \frac{\eta_i''}{\eta_i - \eta_o} - \frac{2[\eta_i' - \eta_o']\eta_i'}{(\eta_i - \eta_o)^2} + \frac{2\sigma[\eta_i' - \eta_o']^2}{(\eta_i - \eta_o)^2}$$

$$- \frac{\sigma[\eta_i'' - \eta_o'']}{\eta_i - \eta_o} + \{[\sigma(\eta_i - \eta_o) + \eta_o](\eta_i - \eta_o)\}^{-1}. \tag{41}$$

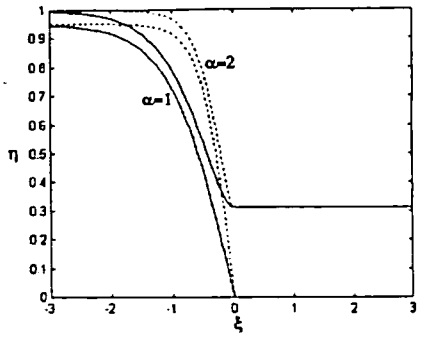

Figure 2.

To solve the problem (34)-(38) we discretize the derivatives using finite differences in a mesh of $\mathcal{M}$ equidistant points along the σ-direction, and $\mathcal{N}$ points in the ξ-direction, resulting a system of $\mathcal{M} \times \mathcal{N}$ algebraic equations for the unknowns $\psi_{m,n}$ on each node (m, n), $1 \le m \le \mathcal{M}$, $1 \le n \le \mathcal{N}$. For the case (a) the system is linear, and is solved using Newton's method. For the cases (b) and (c), the system of algebraic equations is non-linear, and we solved it by Newton's method combined with an iterative method. In all the three cases we use the inlet flow as the initial guess, which makes fastest the convergence of the method. We tried several values of the mesh size, corresponding to $\mathcal{M} \times \mathcal{N} = 100 \times 100$, 200×200, 300×200 and 500×500. Since the results were practically the same for the two latest cases (at least the first four digits were the same), we obviously used a grid of 300×200 points for all the results presented here (more points in the σ-direction than in the ξ-direction are used to have greater accuracy near the inner and outer walls). The end values ξ_1 and ξ_2 must be large enough for the inner and outer walls of the pipe be parallel to the axis of symmetry at the inlet and outlet regions. These values are related to α, that fixes the length of the inner wall in relation to its radius: the appropriate values of ξ_1 and ξ_2 decrease as α increases. Figure 2 shows the pipe geometry for two differents values of α. It is observed that the use of $\xi_1 = 3$ is enough when $\alpha = 2$, but it is not for $\alpha = 1$ ($\xi_2 = 3$ is appropriate in both cases). To be sure that the pipe wall is straight at the inlet and outlet regions for a variety of values of α, we have used $\xi_1 = 10$ and $\xi_2 = 10$ in all the computations reported below. Also, we have fixed $R = 0.95$ and $R_p = \sqrt{1 - R^2} = 0.31225$.

The numerical computations reveal a very different evolution of the flow pattern as L increases

for the three cases considered, as shown in figures 3-5 for $\alpha = 1$.

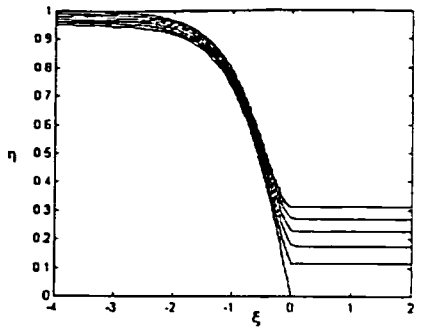

Figure 3(a). Streamlines for the case (a) with $L = 0.5 < L_r^{(a)}$.

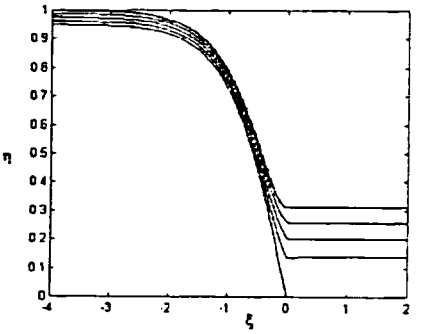

Figure 3(b). Streamlines for the case (b) with $L = 0.25 < L_r^{(b)}$.

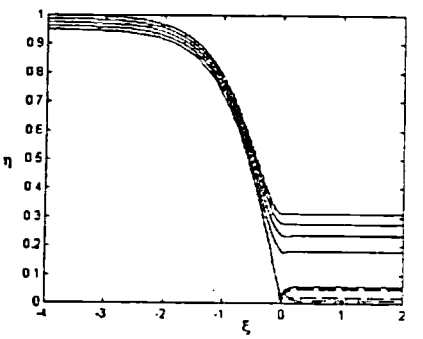

Figure 3(c). Streamlines for the case (c) with $L = 0.2$. Dashed lines correspond to $\psi < 0$.

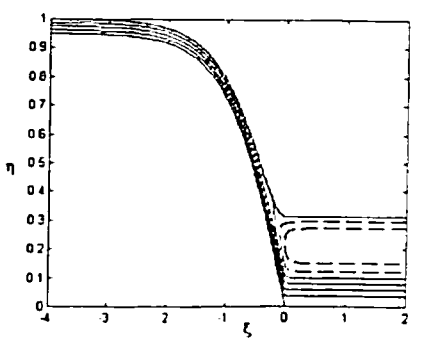

Figure 4(a). Streamlines for the case (a) with $L = 2.0 > L_r$. Dashed lines correspond to reversal flow near the outer wall.

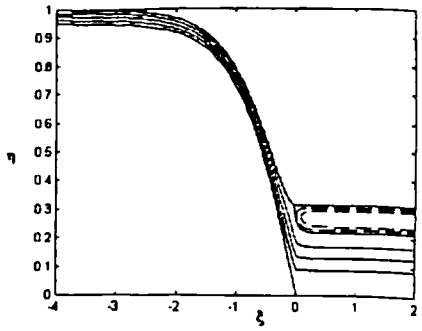

Figure 4(b). Streamlines for the case (b) with $L = 0.45 > L_r^{(b)}$. Dashed lines correspond to reversal flow near the outer wall.

In the cases (a) and (b), the downstream flow changes smoothly as L increases from 0 up to a value L_r, which depends on R and R_p for a given inlet flow. Above L_r, a region of flow reversal is formed near the outer wall. An asymptotic analysis for R_p small shows that L_r for the cases (a) and (b) are given by

$$L_r^{(a)} = \frac{\sqrt{2(1-R)}}{R_p} + \frac{\frac{1}{R} - 1}{2\sqrt{2(1-R)}} R_p + O(R_p^3), \quad (42)$$

$$L_r^{(b)} = \frac{j_{0,1}(1-R^2)}{2R_p} + O(R_p^2(1-R^2)), \quad (43)$$

where $j_{0,1} \simeq 2.4048$ is the first zero of the Bessel function J_0. These expressions are in excellent agreement with the values found numerically (with the present values of R and R_p, $L_r^{(a)} = 1.0387$ and $L_r^{(b)} = 0.3754$). In the case (c), a near-axis region of flow reversal is formed for any value of L, even for $L \to 0^+$. These differences can be observed in figures 3 and 4. As L increases from L_r in the cases (a) and (b), or from zero in the case (c), there exist a second distinguished value of L, L_f, which also depends on R and R_p for a given inlet flow, above which the flow structure changes dramatically, appearing a periodic flow with many bubbles with flow recirculation, as seen in figure 5 for the case (a) (for the other two inlet flows the iterative method does not converge when $L > L_f$). For $L > L_f$ the flow has no longer a cylindrical structure downstream: An asymptotic analysis reveals that there exist a threshold value of L above which the quasi-cylindrical solution breaks down. These asymptotic values are given by

$$(a) \quad L_f^{(a)} = \frac{j_{1,1}}{2R_p},$$

$$(b) \quad L_f^{(b)} = \frac{j_{1,1}(1-R^2)}{2R_p},$$

$$(c) \quad L_f^{(c)} = \frac{j_{1,1}(1-R^2)}{2R_pR^2}. \qquad (46)$$

where $j_{1,1} \simeq 3.8317$ is the first zero of the Bessel function J_1 ($L_f^{(a)}$ is exact, while $L_f^{(b)}$ and $L_f^{(c)}$ are asymptotic for R_p small). These expressions are in excellent agreement with the values found numerically (for the present values of R and R_p, $L_f^{(a)} = 6.1356$, $L_f^{(b)} = 0.5982$, $L_f^{(c)} = 0.6629$).

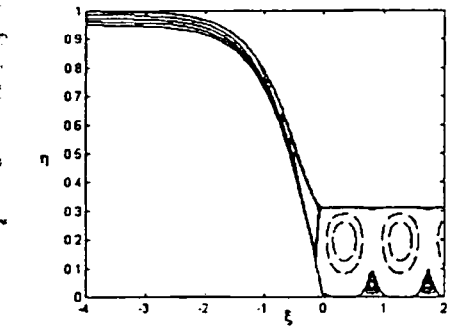

Figure 5. Streamlines for the case (a) with $L = 7.0 > L_f$. Dashed lines correspond to $\psi < 0$.

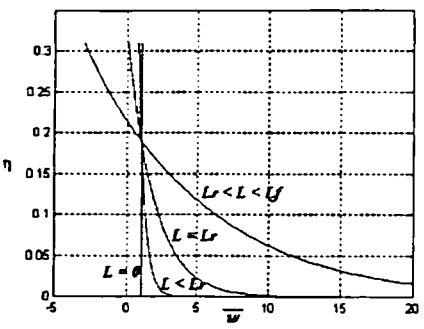

Figure 6. Axial velocity profiles downstream ($\xi_2 = 10$) for several values of L.

In order to better appreciate the transformations in the flow structure as L increases, we show in figure 6 the axial velocity $\overline{w}$ at the pipe outlet corresponding to an inlet flow (a) for different values of L. It is observed that, without rotation ($L = 0$), the velocity is uniform across the outlet section. When the inlet flow rotates, the axial velocity becomes singular near the axis, even for very small values of L. The effect of increasing L is to accelerate the flow near the axis of symmetry and decelerate it near the outer wall, being zero at the wall when $L = L_r$, and becoming negative for $L_r < L \leq L_f$. For $L > L_f$ the outlet flow is no longer cylindrical.

We have seen that, for the third type of inlet flow considered (c), a zone o flow reversal is always formed near the axis for $L > 0$, with the streamline $\psi = 0$ starting at some point in the inner wall (figure 3(c)). It is of interest to know whether this recirculation "bubble" can be separated form the inner wall by changing the pipe geometry, creating an expansion in the downstream flow section. To that end we have considered a different section $\mathcal{S}(\xi)$, with a contraction-expansion region between two given axial locations ξ_a and ξ_b:

$$\mathcal{S}(\xi) = \mathcal{S}_0 \text{ for } -\xi_1 \leq \xi \leq \xi_a, \qquad (47)$$

$$\mathcal{S}(\xi) = \mathcal{S}_0 + \frac{1}{2}\alpha_c(\cos(2\pi\frac{\xi-\xi_a}{\xi_b-\xi_a}) - 1)$$

$$\text{for } \xi_a < \xi \leq \xi_b, \qquad (48)$$

$$\mathcal{S}(\xi) = \mathcal{S}_0 \text{ for } \xi_b < \xi \leq \xi_2. \qquad (49)$$

The pipe interior has thus a minimum section $\mathcal{S}_0 - \alpha_c$ located at $\xi_m = \frac{\xi_b+\xi_a}{2}$. We have tried differents values of ξ_a, ξ_b and α_c, and found that for a contraction-expansion centered at $\xi_m = 0$ (e.g. $\xi_a = -1$ and $\xi_b = +1$), for each value of L there exists a contraction factor $\alpha_c^*(L)$ above which the $\psi = 0$ streamline becomes detached from the inner body. For $\alpha_c > \alpha_c^*(L)$ a stagnation point is thus formed at some location in the axis, and an open bubble of flow reversal is formed after it (see figure 7, where we plot the streamlines for the same case of figure 3(c) with a contraction; $\xi_a = -1$, $\xi_b = 1$ and $\alpha_c = 0.08$).

Finally, we have also considered the influence of the axial characteristic length of the pipe α. In particular, figures 8-10 show the streamlines corresponding to $\alpha = 2$ for an inlet flow of type (a) with three different values of L. One may see that only minor changes are produced in the flow near the region where the inner body ends.

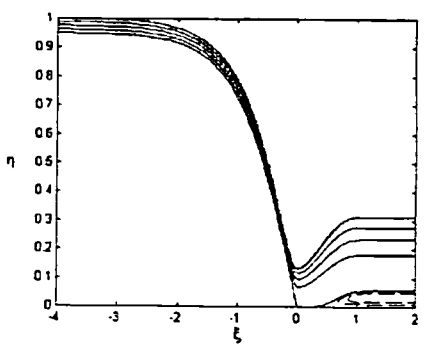

Figure 7. As in figure 3(c) but with a pipe contraction.

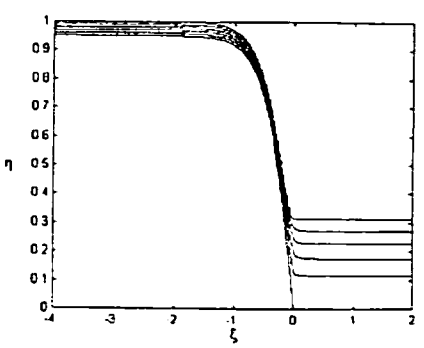

Figure 8. As in figure 3(a) but with $\alpha = 2$.

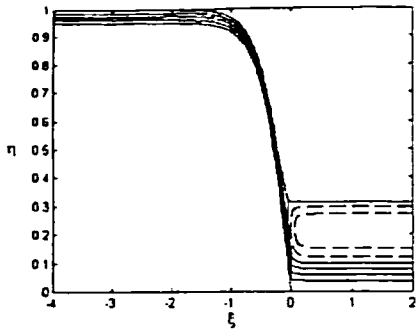

Figure 9. As in figure 4(a) but with $\alpha = 2$.

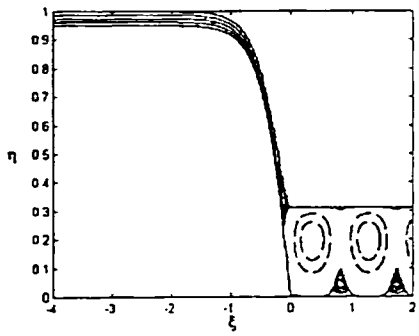

Figure 10. As in figure 5 but with $\alpha = 2$.

Far downstream the flow is, as predicted by the asymptotic analysis, independent of α (see figure 11, where the outlet ($\xi = \xi_2$) axial velocity profiles for $\alpha = 1$ and $\alpha = 2$ are compared).

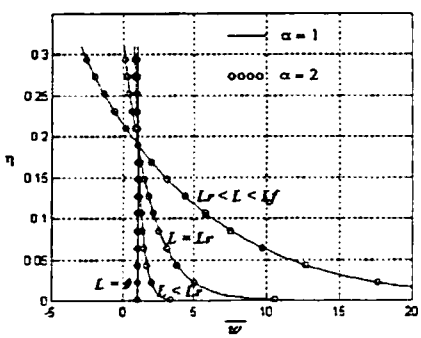

Figure 11. Axial velocity profiles downstream ($\xi_2 = 10$) for $\alpha = 1$ and $\alpha = 2$.

CONCLUSIONS

We have solved numerically the Bragg-Hawthorne equation governing the inviscid evolution of axisymmetric swirling flows in pipes, and find out that the downstream flow depends on the inlet velocity profile not only quantitatively, but also qualitatively. We have seen that the flow structure changes when the inlet swirl parameter L goes across two different threshold values, which depend on the pipe geometry. The numerical results show, in agreement with the asymptotic results, that the pipe geometry dependence of these critical values of the swirl parameter is very different for the three inlet flows considered. In particular, the value L_f above which the downstream flow has no longer a cylindrical symmetry (vortex breakdown) depends strongly on the inlet flow considered. The inlet flow corresponding to an inner body rotation with the outer pipe wall at rest (case (c)) is of particular interest because the inviscid evolution of the flow predicts that an inner (near-axis) bubble with flow recirculation is always present downstream, even for vanishing swirl at the pipe inlet. Also, for this case, the value L_r above which a region of flow reversal near the outer wall is produced downstream is larger than L_f, so that this flow configuration is never reached. In the other two cases considered, $L_r < L_f$, so that, when L increases, a region of flow reversal near the outer wall is always formed before the swirling flow breaks down. All these results show that one has to be cautious before drawing conclusions about the behavior of swirling flows inside pipes from the inviscid equations alone, and that the effect of viscosity should be taken into account in order to predict the breakdown of the flow.

REFERENCES

[1] Z. Rusak and S. Wang, "Review of theoretical approaches to the vortex breakdown phenomenon", AIAA paper 96-2126, 1996.

[2] S. L. Bragg and W. R. Hawthorne, "Some exact solutions of the flow through annular cascade actuator discs", J. Aero. Sci., vol. 17, pp. 243-249, 1950

[3] J. D. Buntine and P. G. Saffman, "Inviscid swirling flows and vortex breakdown", Proc. R. Soc. Lond. A, vol. 449, pp. 139-153, 1995.